Research Article

ADVANCED PHOTONICS

Coherence entropy during propagation through complex media

Xingyuan Lu,[a,†] Zhuoyi Wang,[a,†] Qiwen Zhan,[b,*] Yangjian Cai,[c,d,*] and Chengliang Zhao[a,*]

[a]Soochow University, School of Physical Science and Technology, Jiangsu Key Laboratory of Frontier Material Physics and Devices, Suzhou, China
[b]University of Shanghai for Science and Technology, School of Optical-Electrical and Computer Engineering, Shanghai, China
[c]Shandong Normal University, School of Physics and Electronics, Shandong Provincial Engineering and Technical Center of Light Manipulations, Shandong Provincial Key Laboratory of Optics and Photonic Device, Jinan, China
[d]East China Normal University, Joint Research Center of Light Manipulation Science and Photonic Integrated Chip of East China Normal University and Shandong Normal University, Shanghai, China

Abstract. The deformation, flicker, and drift of a light field owing to complex media such as a turbulent atmosphere have limited its practical applications. Thus, research on invariants in randomly fluctuated light fields has garnered considerable attention in recent years. Coherence is a statistical property of light, while its full and quantitative characterization is challenging. Herein, we successfully realize the orthogonal modal decomposition of partially coherent beams and introduce the application of coherence entropy as a global coherence characteristic of such randomly fluctuated light fields. It is demonstrated that coherence entropy remains consistent during propagation in a unitary system by unraveling complex channels. As representative examples, we study the robustness of coherence entropy for partially coherent beams as they propagate through deformed optical systems and turbulent media. Coherence entropy is anticipated to serve as a key metric for evaluating the propagation of partially coherent beams in complex channels. This study paves the way for a broader application scope of a customized low-coherence light field through nonideal optical systems and complex media.

Keywords: complex media; propagation invariant; modal decomposition; orbital angular momentum; statistical optics; coherence.

Received Mar. 20, 2024; revised manuscript received May 31, 2024; accepted for publication Jun. 4, 2024; published online Jul. 18, 2024.

[DOI: 10.1117/1.AP.6.4.046002]

1 Introduction

In contrast to amplitude, phase, and polarization, coherence is a statistical property of photons that characterizes their phase space occupation.[1–4] Recent research on partially coherent beams has sufficiently demonstrated the versatility of coherence manipulation in various applications, such as higher-resolution speckle-free imaging,[5–7] ghost imaging,[8,9] antiturbulence optical interconnects,[10,11] and the ultimate capability to shape[12] in both macroscopic devices[13,14] and informational photonic systems.[15–17] Passive decoherence is a common phenomenon that occurs when coherent light passes through complex media, which induces random fluctuations. Thus, research on embedded invariants, such as spatial mode[18] and polarization,[19–21] has garnered considerable attention in optical communications and encryptions. Premeditated decoherence and coherence modulation can make the statistical characteristics of the light field serve as an additional information channel.[22]

However, the full characterization of incoherent light fields is challenging. A four-dimensional cross-spectral density or mutual coherence function is required to describe the coherence properties in the quasi-monochromatic case.[1–4] In other words, the full characterization of incoherent light fields requires a four-dimensional measurement. On the detection plane, point-to-point or a complex-valued two-dimensional slice of cross-spectral density can be measured.[23–25] Although full-space reference points scanning may yield complete information, the integrity and reproducibility of this information remain unexplored. A single two-dimensional cross-spectral density slice is not sufficient to characterize a partially coherent beam, and it is also

*Address all correspondence to Qiwen Zhan, qwzhan@usst.edu.cn; Yangjian Cai, yangjian_cai@163.com; Chengliang Zhao, zhaochengliang@suda.edu.cn
†These authors contributed equally to this work.

difficult to achieve orthogonal modal decomposition. Owing to a lack of measurement methods, limited research has been conducted on invariants in the statistical characteristics of light fields.

In this work, we introduce the utilization of coherence entropy, a global coherence characteristic of randomly fluctuated light fields, in the analysis of partially coherent beams generated from orthogonal modes.[26–30] A full four-dimensional characterization of partially coherent light fields was conducted to quantify coherence entropy and demonstrate its robustness during propagation through diverse complex media.[31] Based on theoretical analysis and experimental results, we found that in a unitary channel, the output mode-weights and corresponding coherence entropy can be recovered to be consistent with that on the source plane by utilizing the transmission matrix on source bases. In a turbulent atmosphere, the coherence entropy of a low-coherence beam remains unaltered when the convolution kernel of turbulence is negligible in comparison with the kernel induced by the coherence function. More flexibly, by unraveling complex channels, the coherence entropy could be recovered in turbulent media. The coherence entropy related to the overall mode-weights can also be extended to the vector light source[32–34] with a diagonal beam coherence-polarization matrix based on the assumption that two polarizations construct the same set of orthogonal spatial basis.

2 Theory

A partially coherent light field, which is a randomly fluctuated electric field, is the statistical average of instantaneous electric fields. The cross-spectral density function aids in analyzing second-order statistics,[2] such as the average intensity and degree of coherence when it propagates through complex media. In practical applications, a single slice of four-dimensional cross-spectral density can be measured.[23–25] Such a slice does not adequately reflect the genuine global characteristic of the four-dimensional partially coherent beam, especially for a beam with nonuniform correlation structures or a mode-superposed beam with no specific mathematical model. According to Mercer's theorem,[35] for a continuous, Hermitian, nonnegative definite Hilbert–Schmidt kernel, the cross-spectral density can be reformed using modal decomposition as follows:

$$W_0(\mathbf{r}_1,\mathbf{r}_2)=\sum_N \lambda_n \phi_n^*(\mathbf{r}_1)\phi_n(\mathbf{r}_2), \tag{1}$$

where $\mathbf{r}$ is a source vector coordinate and "*" means conjugate; the frequency is omitted for brevity under the assumption of quasi-monochromatic light. Thus, a partially coherent beam simply means being spatially partially coherent. Here, ϕ_n is an orthogonal eigenfunction with a total number N, and the corresponding coefficient is λ_n, which can be calculated according to the homogeneous Fredholm integral equation $\int W_0(\mathbf{r}_1,\mathbf{r}_2)\phi_n(\mathbf{r}_1)\mathrm{d}\mathbf{r}_1=\lambda_n\phi_n(\mathbf{r}_2)$. For instance, the cross-spectral density may be decomposed into incoherence superposition of a set of Hermite–Gaussian (HG) modes,[36] as shown below,

$$W_0(\mathbf{r}_1,\mathbf{r}_2)=\sum_{m=1}^{N_c}\sum_{n=1}^{N_c}\lambda_{mn}\mathrm{HG}_{mn}^*(\mathbf{r}_1)\mathrm{HG}_{mn}(\mathbf{r}_2), \tag{2}$$

where λ_{mn} is the mode-weight of HG_{mn}, and the total number of HG modes is $N_{\mathrm{total}}=N_c\times N_c$. For a partially coherent beam with a simple model, the theoretical mode-weights were calculated by fitting the beam waist and coherence width, e.g., a Gaussian Shell modal (GSM) beam (see Supplementary Material). The orthogonal basis may be considered a three-dimensional secret key matrix and the mode-weights the password. Such a description contains a high volume of information regarding the partially coherent beam, which can be regarded as a true global description. Statistical properties, such as average intensity and cross-spectral density, can be flexibly reconstructed when required.

We now consider a one-sided unitary optical system with a transmission matrix T (which acts only on spatial distributions), after which the cross-spectral density of the output partially coherent light is expressed as

$$W_T(\boldsymbol{\rho}_1,\boldsymbol{\rho}_2)=\sum_{N'}\lambda_n'\phi_n'^*(\boldsymbol{\rho}_1)\phi_n'(\boldsymbol{\rho}_2), \tag{3}$$

where $\boldsymbol{\rho}$ is the vector coordinate on the output plane. The unitary nature of T preserves the inner products, so the spatial basis $|\phi_n'\rangle=T|\phi_n\rangle$ is still orthogonal as $\langle\phi_n'|\phi_m'\rangle_{m\neq n}=\langle\phi_n|T^\dagger T|\phi_m\rangle_{m\neq n}=\langle\phi_n|\phi_m\rangle_{m\neq n}=0$.[19] For a beam with the given mathematical model, the basis ϕ_n' can be calculated. As an example, the Fraunhofer diffraction (a typical unitary channel) of a GSM beam through a circular lens was derived (see Supplementary Material). In a broader context, the determination of ϕ_n' involves the application of the unitary transmission matrix to the initial ϕ_n, with the preservation of orthogonality ensuring the realization of incoherent modal decomposition. Subsequently, selecting ϕ_n' as the decomposition basis, the mode-weight λ_n' will correspond to the weight of ϕ_n, with its value equal to λ_n. Conversely, the mode-weight varies when an unsuitable spatial basis is selected. Importantly, the calculation of ϕ_n' is closely linked to the transmission matrix T, which includes optical elements, propagation, and turbulence phases.

To quantitatively evaluate the changes of mode-weights in complex media, the coherence entropy was introduced, and defined as[26–30]

$$S=-\sum_{N_{\mathrm{total}}}\lambda_{mn}\log_{N_{\mathrm{total}}}(\lambda_{mn}). \tag{4}$$

The coherence entropy ranges from a minimum value of 0, indicating a fully ordered state where only one mode possesses a weight of 1, to a maximum value of 1, representing the most disordered state characterized by multiple modes with equal weights and no bias. Thus, the value of coherence entropy is contingent upon the relative distribution of mode-weights. It can be utilized to evaluate the robustness of partially coherent light transmission in optical systems and to detect variations in the light field induced by the system. Entropy is a fundamental concept that quantifies the level of disorder. Recent research has explored the connection between information entropy and the spatial coherence width of a partially coherent beam.[16] The presence of disordered phases in a dielectric nanofin array leads to varying sizes of instantaneous intensity speckles. Consequently, a greater amount of information entropy is associated with reduced spatial coherence. Similarly, in the context of modal decomposition, the coherence entropy tends to increase as the coherence width decreases.

3 Results

To experimentally investigate the coherence entropy during propagation, multimode ptychography was employed to reconstruct the full information of the cross-spectral density function, that is $W_0(\mathbf{r}_1,\mathbf{r}_2)=\sum_{t=1}^{M}P_t^*(\mathbf{r}_1)P_t(\mathbf{r}_2)$.[31] $\{P_t(\mathbf{r})\}$ represents the measured mixed modes that are not necessarily orthogonal, and M denotes the total number, which is not necessarily equal to N_{total}. To further calculate the mode-weight for the chosen orthogonal basis, e.g., HG basis, each measured mode was decomposed as $P_t(\mathbf{r})=\sum_{m=1}^{N_c}\sum_{n=1}^{N_c}u_{mnt}\mathrm{HG}_{mn}(\mathbf{r})$. Thus, the cross-spectral density in Eq. (2) was reorganized as

$$W_0(\mathbf{r}_1,\mathbf{r}_2)=\sum_{m=1}^{N_c}\sum_{n=1}^{N_c}\left[\sum_{t=1}^{M}(u_{mnt})^2\right]\mathrm{HG}_{mn}^*(\mathbf{r}_1)\mathrm{HG}_{mn}(\mathbf{r}_2). \tag{5}$$

Therefore, the mode-weight λ_{mn} in Eq. (2) was calculated using

$$\lambda_{mn}=\sum_{t=1}^{M}(u_{mnt})^2, \tag{6}$$

where $u_{mnt}=\int P_t(\mathbf{r})\cdot\mathrm{HG}_{mn}^*(\mathbf{r})\mathrm{d}^2\mathbf{r}$. This means that for any partially coherent beam with a complex or unknown model, the mode-weights matrix λ_{mn} of the chosen orthogonal basis can be obtained using the incoherent modal decomposition with measured mixed modes $\{P_t(\mathbf{r})\}$.

Figure 1 shows a schematic of orthogonal modal decomposition for a GSM beam (see Appendix), whose coherence depends on the beam spot size on the rotating ground glass disk (RGGD). As shown in Part-3, the mixed modes $\{P_t(\mathbf{r})\}$ were reconstructed according to the multimode ptychography iterative engine, whose update function follows Eq. (10). Examples of the reconstructed mixed modes for a low-coherence GSM beam and the diffraction patterns are shown in Fig. 1. Considering a GSM beam and two mode-superposed partially coherent light sources as examples, Fig. S1 in the Supplementary Material shows that the calculated mode-weight of an orthogonal basis (shown in bars) agrees with that actually used for superposition. If only the traditional two-dimensional focal cross-spectral density is measured, the mode-weights cannot be obtained, except for beams with known models and analytical solutions. However, the four-dimensional

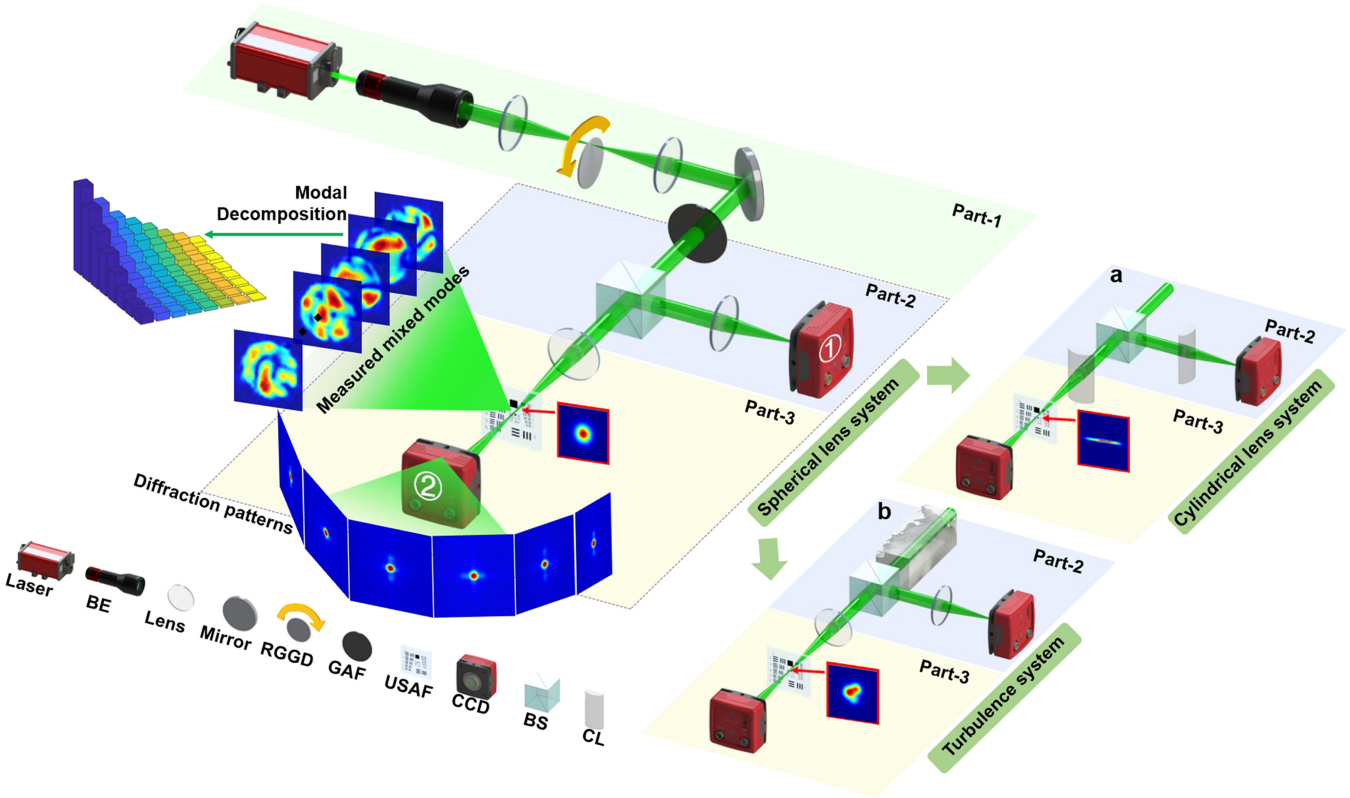

Fig. 1 Schematic diagram of incoherent modal decomposition. Part-1: generation of a partially coherent beam with adjustable coherence width. The coherence width can be modified by shifting the spherical lens before the RGGD back and forth. Part-2: intensity monitor. The GSM beam propagates through a spherical lens system ($f=300$ mm), and CCD1 is used to monitor the intensity distribution. Part-3: modal decomposition. A high-scattering object (USAF) is placed on the measurement plane, and CCD2 is used to obtain the diffraction pattern. The USAF is fixed on a translation stage, and it moves on the transverse plane to take diffraction patterns. The spherical lens system is replaced with (a) a cylindrical lens system and (b) a turbulent atmosphere system for the study of coherence entropy in complex media. The focal length of cylindrical lens is 150 mm. BE, beam expander; GAF, Gaussian amplitude filter; USAF, 1951 USAF resolution test chart; CCD, charge-coupled device; BS, beam splitter; and CL, cylindrical lens.

cross-spectral density measurement results of our modal decomposition method yield complete information and exhibit a high flexibility.

To demonstrate the recovery of mode-weights in deformed systems and the significance of the measurement scheme, we examined a GSM beam passing through a cylindrical lens system. The schematic of this system is shown in Fig. 1(a). In contrast to the GSM beam passing through a spherical lens, the distribution of focal intensity has been elongated after it passes through the cylindrical lens [Figs. 2(a) and 2(b)], and the deformation also occurs on the cross-spectral density distribution. Here, "T" represents the transmission matrix of the cylindrical lens system. If original symmetric HG modes [Fig. 2(c)] defined according to the beam width and coherence width along the short axis are used, the mode-weights of the focused elongated beam [Fig. 2(e)] are not consistent with those of the source GSM beam [Fig. 2(d)]. This is in good agreement with the theoretical analysis (see Supplementary Material). However, when we applied the transmission matrix T on the source orthogonal basis to obtain a new spatial basis [Fig. 2(f)], the mode-weight distribution can be recovered.[37,38] We can capitalize on such flexibility of the measurement scheme for broader applications. Figures 2(g)–2(j) show the mode-weight adjustment of a GSM beam with various degrees of coherence. Here, δ_0 represents coherence length and w_0 represents the beam width. The "before" shown with orange bars means that the mode-weights

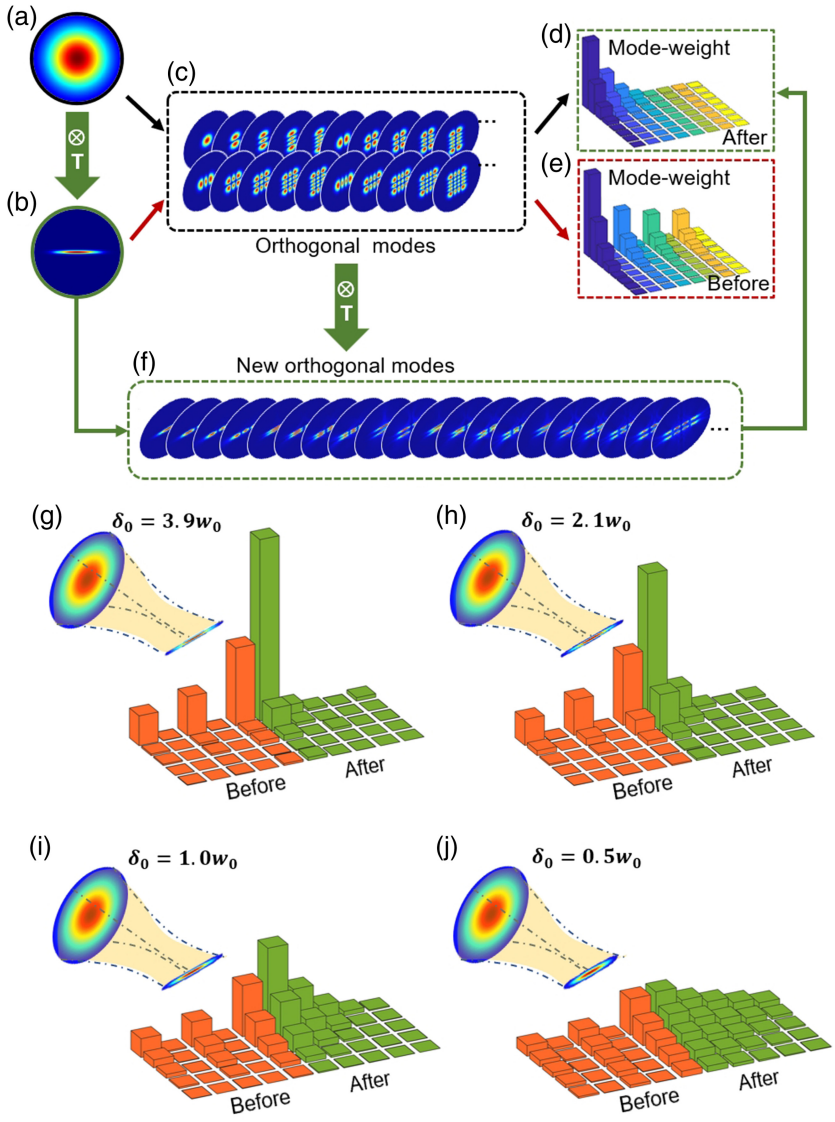

Fig. 2 Basis adjustment for modal decomposition. (a) A GSM beam in the source plane and (b) the elongated beam spot after going through a cylindrical lens system. Using the symmetric HG basis, mode-weight results in panels (d) and (e) are calculated for (a) and (b), respectively. (f) Basis after applying the transmission matrix on panel (c), which helps recover the mode-weights. (g)–(j) Mode-weight distributions of a GSM beam propagating through a cylindrical lens for various coherent widths. The orange bars correspond to the mode-weight distribution before adjusting the orthogonal basis, and the green bars show the mode-weights after adjusting the orthogonal basis. Here, only the main part (5×5) of the mode-weight distribution (8×8 in total) is displayed.

were calculated according to a symmetrically distributed HG basis, and the "after" (green bars) means that the mode-weights were adjusted by applying the transmission matrix on the source orthogonal basis. After basis adjustment, the mode-weight can be corrected to be consistent with that of the source plane for both high- and low-coherence cases.

To further illustrate that coherence entropy can be recovered in deformed systems, theoretical mode-weights and their corresponding coherence entropies were simulated for a GSM beam passing through a cylindrical lens system, as shown in Table 1. The row labeled "GSM source" shows the dependence of coherence entropy on coherence width. The lower the coherence width, the higher the coherence entropy. After passing through the cylindrical lens system, if the spatial basis is not suitable, the computed coherence entropy will deviate from the coherence entropy of the source. The last row shows the results obtained after basis adjusting by applying the transmission matrix on the source basis. It shows that the coherence entropy can be recovered.

In comparison to static systems, the complexity of the transmission matrix in turbulent media is heightened. When a GSM beam passes through the turbulent atmosphere, the intensity captured by the camera drifts and deforms constantly. Figure 3 shows the mode-weight results of a GSM beam with three coherence widths passing through a turbulent atmosphere generated using a temperature-adjustable hot plate. The low-turbulence atmosphere in Figs. 3(a)–3(c) corresponds to room temperature, and the high-turbulence atmosphere in Figs. 3(d)–3(f) corresponds to 200°C. The coherence length δ_0 was determined to be $4.35w_0$ for high coherence, $1.58w_0$ for medium coherence, and $0.34w_0$ for low coherence (see Appendix). Figures 3(g)–3(i) show the difference between the mode-weight matrices of these two turbulence cases. As the coherence width decreases, the mode-weight profile expands, owing to the broadening of the beam and degradation in coherence induced by turbulence. However, a comparison of the first and second rows shows that the fluctuation of mode-weights decreases with the coherence.

Figures 3(j)–3(l) provide a quantitative analysis of the propagation robustness by assessing the coherence entropy of a GSM beam as it propagates through turbulent atmosphere. Three coherence and three turbulence cases were compared. For each parameter setting, 10 sets of data were analyzed. The bars in blue, yellow, and red correspond to the mean values of coherence entropy, with the hot plate set at room temperature (low turbulence), 100°C (medium turbulence), and 200°C (high turbulence). The corresponding beam drift in Fig. S5 in the Supplementary Material shows the effect of the turbulent atmosphere generated using the hot plate. For the high-coherence case, the beam may drift out of the region defined by the beam width at a turbulence of 200°C. As shown in Figs. 3(j)–3(l), for the low-turbulence case (blue bars), as the coherence decreases, the height of the blue bar increases, which indicates an increase in coherence entropy. For medium-turbulence (yellow bars) and high-turbulence (red bars) cases, the coherence entropy is higher than that for the low-turbulence case. This is attributed to the broadening of mode-weights. Although the coherence entropy increases as the turbulence becomes stronger, for a low-coherence beam, the coherence entropy is nearly constant for various turbulence cases. Furthermore, the standard deviation of coherent entropy is represented by the black lines on the bars. The stronger the turbulence, the larger the standard deviation. Compared with the high- and medium-coherence cases, the coherence entropy for a low-coherence beam is more robust to the turbulent atmosphere.

As illustrated in previous research,[39] for a Schell-model light source passing through a random medium (linear, isotropic, and homogeneous), the spectral density is the convolution of the three terms, written as $S(\boldsymbol{\rho}, z) = S_f \otimes p_1 \otimes p_2$. Here, $\otimes$ means convolution, S_f is the spectral density of the coherent portion at a distance z, and p_1 and p_2 are the Fourier transforms of the source degree of coherence and second-order complex phase correlation function of the random medium, respectively. The size of kernels of p_1 and p_2 can be estimated from Figs. 3(c) and 3(d), respectively. The kernel of p_2 can be neglected when the size is considerably smaller than the kernel p_1. It corresponds to a light source with lower coherence, where the impact of turbulence is mitigated to some extent due to the discrepancy between the broadening caused by turbulence and the profile of the mode-weights. Similar results can be seen in Figs. 2(g)–2(j), and the mode-weights of low-coherence light are more robust to complex systems than that of high-coherence light before basis adjustment. However, a trade-off must be considered in this context: as coherence decreases, the number of modes in the light fields increases, leading to increased complexity in modal decomposition experiments.

When the turbulent transmission matrix is determined or measured, the examination of mode-weights and coherence entropy in turbulent media becomes more flexible through the use of basis adjustment, facilitating applications in information coding and robustness evaluation. Additionally, to showcase the versatility of the proposed modal decomposition approach across different bases, experiments involving orbital angular momentum (OAM) multiplexing,[18,40,41] and decomposition were conducted. With traditional demultiplexing methods, the broadening of the OAM spectrum induced by propagation through complex media has not been sufficiently addressed. To solve this problem, we demonstrate the improvement in OAM-based optical encryption and decryption through complex media using basis adjustment (Fig. 4). The multifocal array consisting of various integer vortices[42] is widely used for OAM demultiplexing. A comparison of the regular OAM demultiplexing in free space based on incoherent decomposition with Laguerre–Gaussian basis (see Appendix) and a multifocal array is given in Figs. 4(a) and 4(b). The phase distortion induced by turbulent media [see Fig. 4(c)] was simulated using Zernike polynomials.[43] Consequently, the OAM demultiplexing through turbulent

Table 1 Theoretical simulation of GSM coherence entropy before and after basis adjustment.

	$\delta_0 = 4w_0$	$\delta_0 = 2w_0$	$\delta_0 = 1w_0$	$\delta_0 = 0.5w_0$
GSM source	0.1094	0.2657	0.5142	0.7777
With inappropriate basis	0.3615	0.4424	0.5816	0.7645
After basis adjustment	0.1092	0.2640	0.5139	0.7777

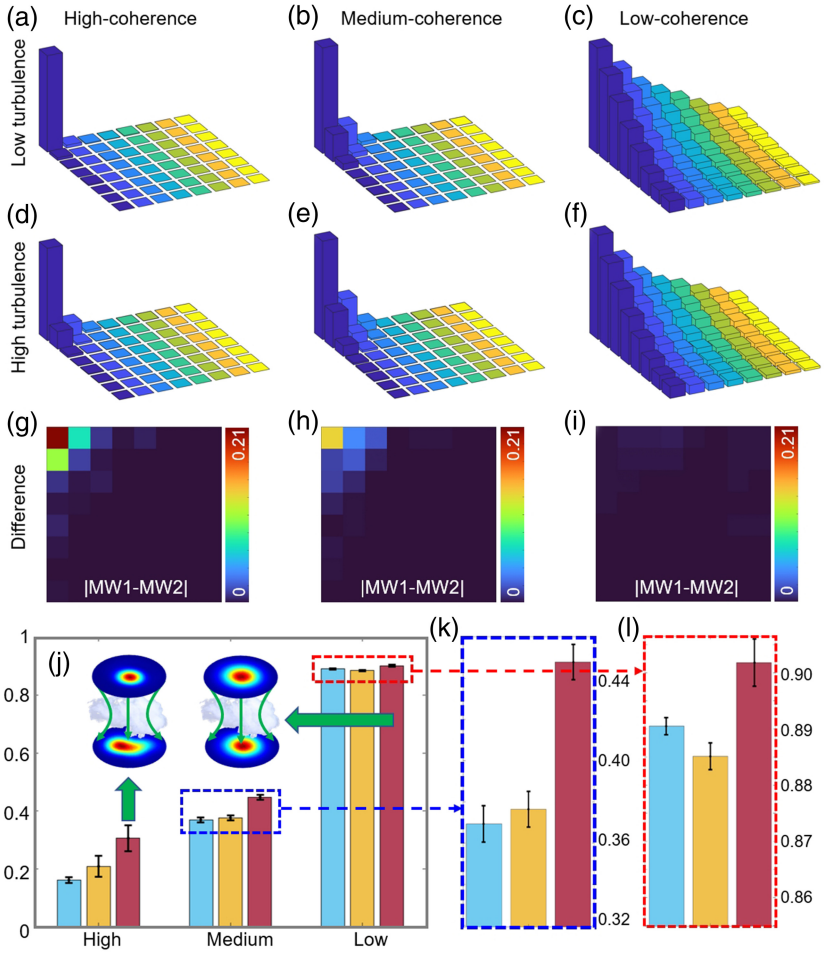

Fig. 3 Coherence entropy of a GSM beam passing through the turbulent atmosphere. The mode-weights for a GSM beam propagating through (a)–(c) low turbulence (MW_1) and (d)–(f) high turbulence (MW_2) atmosphere. (g)–(i) The differences in mode-weights ($|MW_1 - MW_2|$) for two turbulence cases. A low-turbulence atmosphere corresponds to room temperature; a high-turbulence atmosphere is realized by a hot plate at 200°C. (j)–(l) Coherence entropy calculated from mode-weights. (k) and (l) Zoomed-in field of view of the medium-coherence and low-coherence cases. Illustrations in panel (j) show the two intensity deformations caused by a turbulent atmosphere. The deformation is less apparent for lower-coherence case. The blue, yellow, and red bars correspond to the mean value of coherence entropy, under low-, medium-, and high-turbulence atmospheres, respectively. The black error bar shows the standard deviation of 10 data sets.

media became chaotic for both cases, as shown in Figs. 4(d)–4(f). The application of the unitary transmission matrix incorporating the perturbation phase on the source orthogonal bases results in the preservation of orthogonality in the output bases, as demonstrated in Fig. S6 in the Supplementary Material. Subsequently, OAM demultiplexing after propagation through turbulent media can be achieved through incoherent decomposition. For example, an input binary number series "001101011-011100111" was decrypted based on a threshold of 0.25 when reading the normalized mode-weight distribution in Fig. 4(f). Similarly, a string of clock-style numbers "215006" was encrypted using OAM multiplexing; its coding correspondence is shown in Fig. 4(g). Traditional multifocal arrays cannot decrypt such information [see Fig. 4(h) and corresponding simulation results in Fig. S7 in the Supplementary Material]. However, the decryption can be successfully performed after applying basis adjustment in incoherent decomposition.

Furthermore, the coherence entropy proposed in this study defined using an OAM mode-weight matrix may prove instrumental in OAM-based optical communications through complex media.[44,45] In addition, the evaluation of random fluctuations induced by the light source or optical system is no longer limited to the beam shape or other two-dimensional attributes. To demonstrate this, we performed a channel robustness experiment based on the conservation of coherence entropy (Fig. 5). Mode-weights depicted in Fig. 5(a) and Figs. 5(b) and 5(c) were calculated for a focal system in the absence and presence of turbulent media, respectively. In Figs. 5(a) and 5(b), the decomposition bases utilized on the output plane were determined by applying only the transmission matrix of focused propagation on the Laguerre–Gaussian bases. Conversely, in Fig. 5(c), the turbulence phase was taken into account in the transmission matrix and basis calculation. The inset intensity patterns were captured at a focal plane that showed the distortion

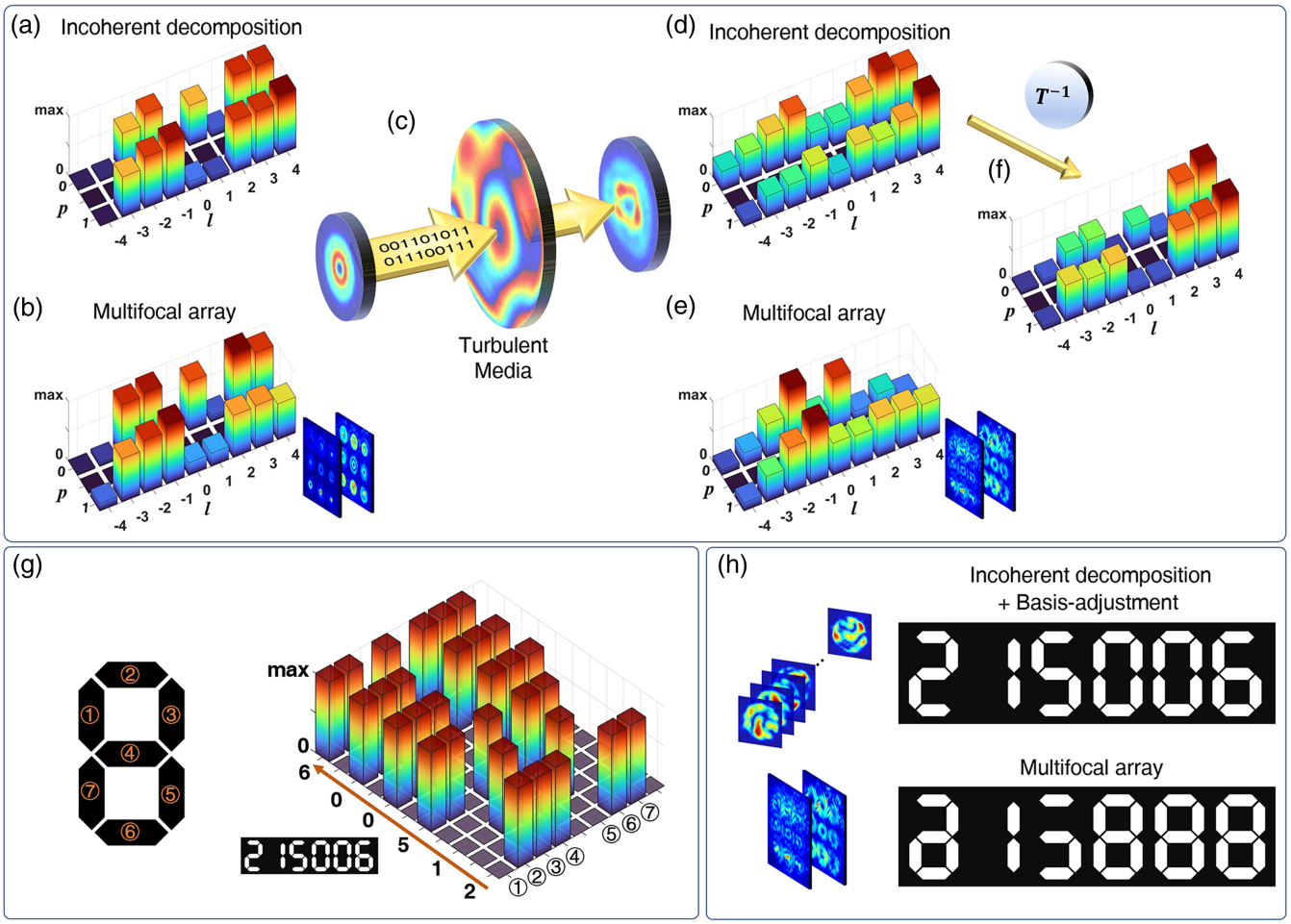

Fig. 4 Performance improvement in OAM-based optical encryption and decryption through turbulent media using basis adjustment. OAM demultiplexing in free-space using (a) incoherent decomposition and (b) traditional multifocal array consisting of different integer vortices. (c) Wavefront distortion induced by the turbulent media. Chaotic OAM demultiplexing through turbulent media using (d) orthogonal modal decomposition and (e) traditional multifocal array. (f) Corrected OAM demultiplexing through turbulent media using mode adjustment for incoherent decomposition. (g) Encryption of a clock-style number string "215006." (h) Experimental demonstration showing that the correct decryption may be achieved after applying mode adjustment in incoherent decomposition, while the traditional method yields highly inaccurate results.

effects owing to the turbulent media. After applying basis adjustment, the mode-weights were corrected from Figs. 5(b) and 5(c); the reconstructed intensity is shown in Fig. 5(c) (see corresponding HG decomposition in Fig. S8 in the Supplementary Material). In Fig. 5(d), the measured coherence entropy without turbulence is highlighted using a black line. A blue dashed line and orange circles correspond to the coherence entropy through turbulent media and corrected coherence entropy after basis adjustment, respectively. A simple demonstration of encoding, which leverages the conservation coherence entropy, is shown in Figs. 5(e)–5(g). The correspondence between colors and the values of coherence entropy is shown in Fig. 5(d). Given that the intensity is highly chaotic after a light beam passes through turbulent media, the input values of coherence entropy drastically increased. Consequently, the color information of architectural images was scrambled [Fig. 5(f)]. However, owing to the conservation of coherence entropy, the correct image could be reconstructed, as shown in Fig. 5(g). The retrieval of information benefits from the precise feedback of the channel transmission matrix. Consequently, when the system encounters unforeseen perturbations, the coherence entropy will fluctuate, indicating the instability of the system.

4 Discussions and Conclusions

This study examines the coherence entropy as defined by the mode-weights of orthogonal bases within partially coherent light fields. The use of orthogonal modal decomposition allows for an exploration of the propagation robustness of coherence entropy within a unitary system, encompassing both static and turbulent media. Our findings demonstrate the recovery of coherence entropy through the unraveling of complex channels and the selection of appropriate bases. The recovery of both mode-weight and coherence entropy is closely linked to the principle of energy conservation. Therefore, in the event that

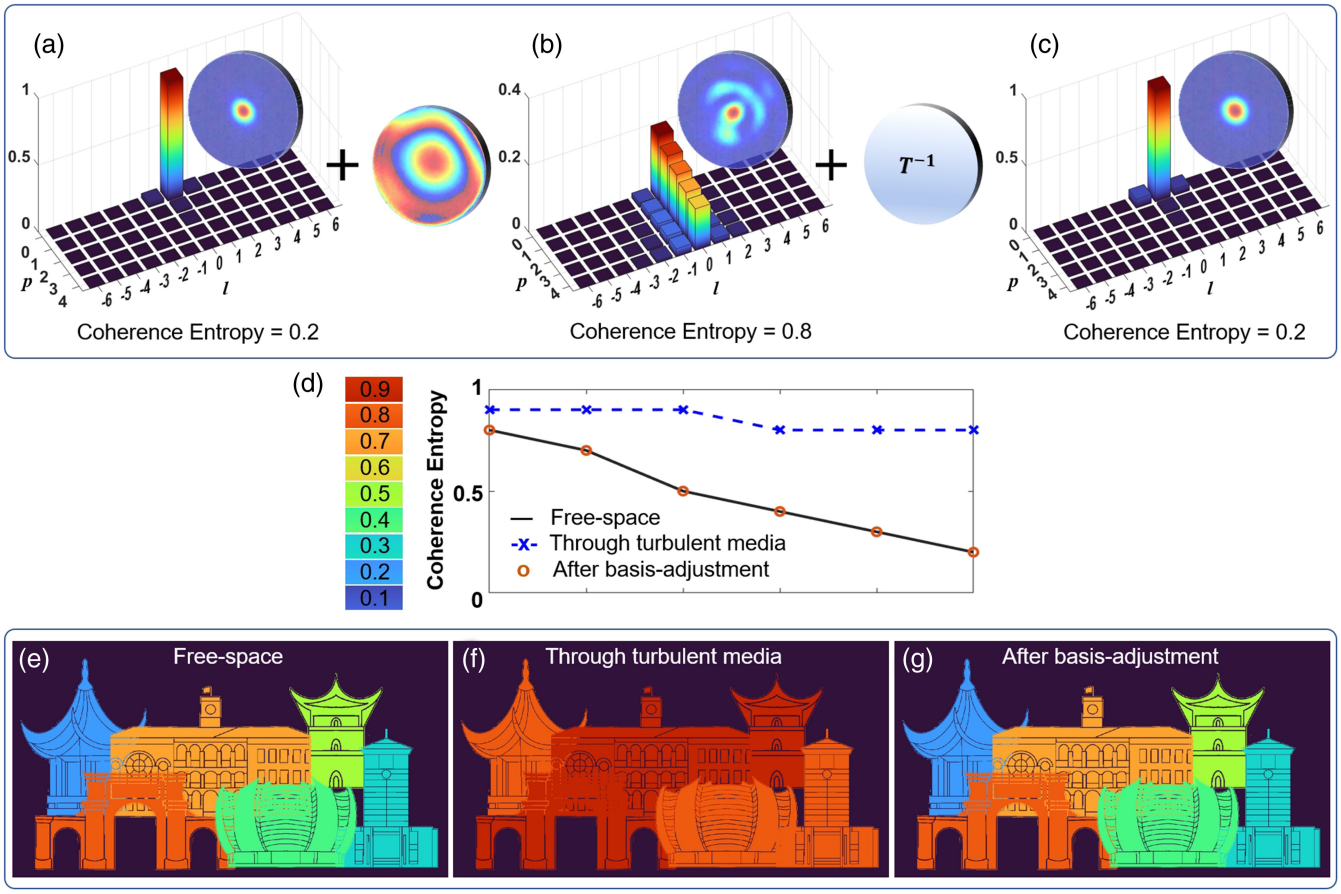

Fig. 5 Channel robustness evaluation using the coherence entropy. Mode-weight distribution (a) in free space and (b) through turbulent media. Inset intensity patterns show the distortion effect caused by turbulent media. The mode-weights and corresponding reconstructed intensity are shown in panel (c). T^{-1} refers to the process of mode adjustment. (d) Measured coherence entropy in free-space (black line), through turbulent media (blue dashed line), and after mode adjustment (orange circles). Channel robustness that leverages the conservation of coherence entropy is demonstrated by sending a color-encoded image through the turbulent media, as shown in panels (e)–(g), with the correspondence between colors and values of coherence entropy shown in panel (d).

absorption is distributed evenly among all modes, the relative distribution of mode-weights and corresponding coherence entropy will remain unchanged. Conversely, if absorption is not uniform, the coherent entropy will be altered. Given the susceptibility of coherent entropy to changes in mode weights and basis selection, this metric can be utilized to evaluate the robustness of the optical system. The existing approach for detecting coherence entropy is reliant on the chosen basis, and the development of a basis-independent detection method could enhance the applicability of coherence entropy in various fields.

However, it is noteworthy that the coherence entropy, as defined by the mode-weights of a nonorthogonal basis, may not necessarily be retrievable. An interesting example is the van Cittert–Zernike theorem (no energy loss), wherein the modes undergo a Fourier transform, i.e., a typical unitary channel. We discuss an incoherent source with equal mode-weights, i.e., $S = 1$. Following the Fourier theorem, on the output plane, a partially coherent light beam can be obtained (nonequal mode-weights). This result may indicate a decreased entropy in a unitary system. However, each mode on the output plane corresponds to a plane wave with a certain tilted phase, which is not an orthogonal mode. Thus, the entropy defined according to these mode-weights is not included in our analysis. The analysis of coherence entropy can be extended to a vector beam with diagonal beam coherence-polarization matrix based on the assumption that the two initial polarization components share the same set of orthogonal spatial basis (see Supplementary Material). The modal decomposition of diagonal coherence-polarization matrix can be simplified as that of a scalar cross-spectral density defined with $W_{\mathrm{eq}} = W_{xx} + W_{yy}$.[33] Thus, the overall mode-weights and corresponding coherence entropy for such a vector partially coherent beam in a unitary system can be reconstructed by selecting appropriate decomposition bases.

Owing to the random fluctuations in turbulence, the coherence entropy carried by high-coherence light increases as it propagates through these media. The variation in coherence entropy increases with the turbulence strength. Without basis adjustment, light fields with lower coherence are more robust to turbulence in terms of coherence entropy. Turbulence can also be described as a set of phase screens and propagation

(slicing up a thick medium), both of which are unitary. The product of unitary matrices is also unitary. Then, the application of the transmission matrix to the selection of orthogonal bases offers a more flexible and accurate approach to studying the robustness of coherence entropy in turbulent media. The coherence entropy, as a global characteristic, is expected to become a key metric for evaluating the propagation of partially coherent beams through complex media with broader practical application prospects.

5 Appendix: Methods

5.1 Theoretical Calculation of Mode-Weights

According to the literature,[1,2] the cross-spectral density function $W_0(\mathbf{r}_1,\mathbf{r}_2)$ may be decomposed as $W_0(\mathbf{r}_1,\mathbf{r}_2)=\sum_{m=1}^{N_c}\sum_{n=1}^{N_c}\lambda_{mn}\phi_{mn}^*(\mathbf{r}_1)\phi_{mn}(\mathbf{r}_2)$. Here, λ_{mn} represents the mode-weights of the mode, ϕ_{mn} represents eigenfunctions orthogonal to each other, and $N_{\text{total}}=N_c\times N_c$ is the number of orthogonal eigenfunctions. Considering a GSM beam as an example, by solving the homogenous Fredholm integral equation $\int W_0(\mathbf{r}_1,\mathbf{r}_2)\phi_{mn}(\mathbf{r}_1)\mathrm{d}\mathbf{r}_1=\lambda_{mn}\phi_{mn}(\mathbf{r}_2)$, the cross-spectral density may be decomposed into the incoherent superposition of HG modes[36] and

$$\begin{aligned}\phi_{mn}(\mathbf{r})&=\left(\frac{2c}{\pi}\right)^{1/2}\frac{1}{\sqrt{2^{m+n}m!n!}}H_m\left(x\sqrt{2c}\right)H_n\left(y\sqrt{2c}\right)\\&\quad\cdot\exp[-c(x^2+y^2)],\\\lambda_{mn}&=\left(\frac{\pi}{a+b+c}\right)\left(\frac{b}{a+b+c}\right)^{m+n},\end{aligned}\tag{7}$$

where $a=1/4w_0^2$, $b=1/2\delta_0^2$, $c=(a^2+2ab)^{1/2}$. H_m and H_n represent mth-order and nth-order Hermite polynomials, respectively. Another example of orthogonal basis is the Laguerre–Gaussian function,[46]

$$\begin{aligned}\phi_{pl}(\mathbf{r})&=\left(\frac{2c}{\pi}\right)^{1/2}\sqrt{\frac{p!}{(p+|l|)!}}\left(\sqrt{2c}\mathbf{r}\right)^{|l|}L_p^{|l|}(2c\mathbf{r}^2)\\&\quad\cdot\exp(-c\mathbf{r}^2)\exp(il\theta),\\\lambda_{pl}&=\frac{\pi}{2c}(1-\epsilon)\epsilon^{\frac{|l|}{2}+p},\quad\epsilon=\frac{a+b-c}{a+b+c},\end{aligned}\tag{8}$$

where L_p^l is the Laguerre polynomial, with p and l being the radial and azimuthal indices, respectively. Therefore, for a GSM beam, provided that the beam waist w_0 and coherence width δ_0 are known, the theoretical mode-weights can be calculated. In addition, the mode-weights remain unchanged when GSM beam passes through a spherical lens. Thus, the cross-spectral density of a GSM beam on the focal plane can be written as $W_f(\boldsymbol{\rho}_1,\boldsymbol{\rho}_2)=\sum_{m=1}^{N_c}\sum_{n=1}^{N_c}\lambda_{mn}\phi_{fmn}^*(\boldsymbol{\rho}_1)\phi_{fmn}(\boldsymbol{\rho}_2)$, where ϕ_{fmn} are the eigenmodes in the focal plane that can be determined according to the focal beam width and focal coherence width, and λ_{mn} remains constant compared to that in the source plane. Strictly speaking, the upper limit of the sum N_c should tend to infinity before a GSM beam can be accurately represented by a polynomial. However, the λ_{mn} gradually decreases to zero with an increase in the order. Therefore, it can also be approximated by considering finite sums.[36]

5.2 Experimental Generation of a Partially Coherent Light Source

As shown in Fig. 1, Part-1 shows the generation of a GSM beam according to the adjustable coherent width. The coherent light emitted from a semiconductor laser (VentusHR, wavelength $\lambda=532$ nm) is expanded by a beam expander (BE) and then focused by a spherical lens (focal length $f_1=100$ mm) onto the RGGD. The scattered light is collimated by the second spherical lens ($f_2=250$ mm) and shaped by a Gaussian amplitude filter (GAF, 1-mm beam waist). After the GAF, a GSM beam with an adjustable coherence is obtained. The coherence width may be modified by shifting the first spherical lens before rotating the RGGD back and forth. The larger the beam spot, the lower the coherence. For convenience, the GAF can also be replaced with a spatial light modulator or digital micromirror device. Part-2 shows the intensity monitor of GSM propagating through spherical lens system ($f_3=300$ mm). The first camera (CCD1, ECO445 SVS-VISTEK, 1296 pixels × 964 pixels, 3.75 μm) is located on the focal plane of the spherical lens. The coherence widths in Fig. 3 correspond to $\delta_0=4.35w_0$ (high coherence), $\delta_0=1.58w_0$ (medium coherence), and $\delta_0=0.34w_0$ (low coherence).

5.3 Experimental Measurement of Mode-Weights

In Fig. 1, Part-3 is used to measure the mixed modes of the GSM beam. The GSM beam that is to be measured illuminates a high-scattering object (1951 USAF resolution test chart), and the second camera (CCD2, Electron-Multiplying CCD, iXon Life Oxford, 1024 pixels × 1024 pixels, 13 μm) is placed at a distance of 146 mm after the object to take the diffraction patterns. To obtain a higher volume of information for reconstruction, a two-dimensional translation stage (CONEX-MFACC Newport) is used to scan the USAF for ptychographic data acquisition. The focal spot is approximately 200-μm wide, and the step size is 40 μm. Finally, the mixed modes and sample information are reconstructed using a multimode ptychography engine.[31] The cross-spectral density and mode-weights may then be calculated further.

For the partially coherent beam with a known model, e.g., GSM, the mode-weights can be calculated using the analytical solution, e.g., Eq. (7). Here, we introduced a model-independent mode-weight measurement method that is suitable for more general partially coherent beams. The characteristics of the partially coherent beam are evident once the propagation or scattering occurs. Therefore, coherent diffraction imaging is used to reconstruct the complete four-dimensional cross-spectral density function of a partially coherent beam. To improve the redundancy of information in the diffraction pattern, which is the key to the convergence of iterative algorithm, a high-scattering object (USAF) is placed between the beam and camera (see Fig. 1). In the conventional coherent diffraction imaging (CDI) device, the beam acts as a probe, and the object is the target to be reconstructed. Here, although the target of the measurement is the light source, we can still use the procedure of CDI. Given that the oversampling ratio should be larger than 2,[47] one diffraction pattern is not sufficient to reconstruct the mixed modes of the GSM. Therefore, a ptychographic scanning is performed.

The purpose of the CDI iterative algorithm is to minimize the difference of collected intensity and calculated average-intensity or the output field $\psi(\boldsymbol{\rho})$ right behind the object plane.

For instance, in the coherence case (i.e., single-mode case), one must solve $\min \|\psi(\boldsymbol{\rho}) - P(\boldsymbol{\rho}) \cdot O(\boldsymbol{\rho})\|^2$. Here, $P(\boldsymbol{\rho})$ is the probe, and $O(\boldsymbol{\rho})$ is the object. The partially coherent beam is the superposition of multimodes, and thus, the problem should be transformed into minimizing collected intensity I_{ccd} and summation of calculated intensity of each mode. Subsequently, each single diffraction field can be renewed with I_{ccd} as[48]

$$\Psi'^{i}_{t,j}(\mathbf{k}) = \left(\sqrt{I_{j\_\text{ccd}}(\mathbf{k})} \Big/ \sqrt{\sum_{M} |\Psi^{i}_{t,j}(\mathbf{k})|^2}\right) \Psi^{i}_{t,j}(\mathbf{k}), \tag{9}$$

where t refers to the tth mode; M is the total number of modes in the partially coherent beam; i represents the ith iteration number; j represents the jth scanning position; I_{j_ccd} denotes the jth collected intensity; and $\boldsymbol{\rho}$ and $\mathbf{k}$ are the coordinates of object and camera planes, respectively. Here, $\psi(\boldsymbol{\rho}) = \mathcal{F}^{-1}\{\Psi'_{t,j}(\mathbf{k})\}$. According to the gradient descent algorithm,[48] the object and probe can be updated using the following equation:

$$\begin{aligned} O^{i+1}_{j}(\boldsymbol{\rho}) &= O^{i}_{j}(\boldsymbol{\rho}) + \alpha \frac{P^{*i}_{t,j}(\boldsymbol{\rho})}{|P^{i}_{t,j}(\boldsymbol{\rho})|^2_{\max}} [\psi'^{i}_{t,j}(\boldsymbol{\rho}) - \psi^{i}_{t,j}(\boldsymbol{\rho})], \\ P^{i+1}_{t,j}(\boldsymbol{\rho}) &= P^{i}_{t,j}(\boldsymbol{\rho}) + \beta \frac{O^{*i}_{j}(\boldsymbol{\rho})}{|O^{i}_{j}(\boldsymbol{\rho})|^2_{\max}} [\psi'^{i}_{t,j}(\boldsymbol{\rho}) - \psi^{i}_{t,j}(\boldsymbol{\rho})], \end{aligned} \tag{10}$$

where α and β are the update factors. The final P_t represents the modes that are reconstructed from the collected diffractive intensities, whose resolution is limited by the ptychography retrieval algorithm that is twice the pixel size. Here, the pixel size defined with $\lambda z/D$ equals 6 μm,[48] $\lambda = 532$ nm is the wavelength, $z = 146$ mm is the distance from the sample to the camera, and $D = 13$ mm is the actual lateral size of camera. Then, the cross-spectral density of the GSM beam on the focal plane can be calculated using $W_f(\boldsymbol{\rho}_1, \boldsymbol{\rho}_2) = \sum_{t=1}^{M} P^*_t(\boldsymbol{\rho}_1) P_t(\boldsymbol{\rho}_2)$. However, $P_t(\boldsymbol{\rho})$ is not orthogonal but a random mode.[25] To calculate the mode-weights for the chosen engine modes (e.g., HG modes), each probe mode is further decomposed using HG basis as $P_t(\boldsymbol{\rho}) = \sum_{m=1}^{N_c} \sum_{n=1}^{N_c} u_{mnt} \text{HG}_{mn}(\boldsymbol{\rho})$. Thus, the focal cross-spectral density may be reorganized as $W_f(\boldsymbol{\rho}_1, \boldsymbol{\rho}_2) = \sum_{m=1}^{N_c} \sum_{n=1}^{N_c} [\sum_{t=1}^{M} (u_{mnt})^2] \text{HG}^*_{mn}(\boldsymbol{\rho}_1) \text{HG}_{mn}(\boldsymbol{\rho}_2)$. Therefore, the mode-weights can be calculated as $\lambda_{mn} = \sum_{t=1}^{M} (u_{mnt})^2$, where $u_{mnt} = \int P_t(\boldsymbol{\rho}) \cdot \text{HG}^*_{mn}(\boldsymbol{\rho}) \text{d}^2\boldsymbol{\rho}$.

Regarding the error of modal decomposition, the upper limit of the sum N_c should tend to infinity. For the partially coherent beam with a known model and analytical solution of mode-weights or the mode-superposed beam, the orthogonal basis may be easily determined. However, for a totally random partially coherent beam, the basis is difficult to choose, and the error of finite decomposition modes increases. Nevertheless, we still emphasize that the scheme of the proposed modal decomposition is flexible, especially when dealing with beams superimposed by orthogonal modes.

Code and Data Availability

Code, data, and materials are available on request from the corresponding author.

Author Contributions

X.L., C.Z., and Q.Z. proposed the original idea and performed the theoretical analysis. X.L and Z.W. performed the experiments and data analysis and contributed to development of the measurement method. C.Z., Y.C, and Q.Z. supervised the project. All the authors contributed to the data analysis and writing of the manuscript.

Acknowledgments

This work was supported by the National Key Research and Development Program of China (Grant Nos. 2022YFA1404800 and 2019YFA0705000); the National Natural Science Foundation of China (Grant Nos. 12174280, 12204340, 12192254, 92250304, and 92050202); the China Postdoctoral Science Foundation (Grant No. 2022M722325); the Priority Academic Program Development of Jiangsu Higher Education Institutions; and the Key Lab of Modern Optical Technologies of Jiangsu Province (Grant No. KJS2138).

References

1. E. Wolf, *Introduction to the Theory of Coherence and Polarization of Light*, Cambridge University Press (2007).
2. E. Wolf, "New theory of partial coherence in the space frequency domain - Part I," *J. Opt. Soc. Am.* **72**, 343–351 (1982).
3. G. Gbur and T. D. Visser, "The structure of partially coherent fields," *Prog. Opt.* **55**, 285–341 (2010).
4. J. W. Goodman, *Statistical Optics*, John Wiley (2015).
5. Y. Peng et al., "Speckle-free holography with partially coherent light sources and camera-in-the-loop calibration," *Sci. Adv.* **7**, eabg5040 (2021).
6. B. Redding, M. A. Choma, and H. Cao, "Speckle-free laser imaging using random laser illumination," *Nat. Photonics* **6**, 355–359 (2012).
7. S. Knitter et al., "Coherence switching of a degenerate VECSEL for multimodality imaging," *Optica* **3**, 403–406 (2016).
8. A. M. Paniagua-Diaz et al., "Blind ghost imaging," *Optica* **6**, 460–464 (2019).
9. Y. Cai and S. Y. Zhu, "Ghost imaging with incoherent and partially coherent light radiation," *Phys. Rev. E* **71**, 056607 (2005).
10. G. Gbur, "Partially coherent beam propagation in atmospheric turbulence," *J. Opt. Soc. Am. A* **31**, 2038–2045 (2014).
11. Y. Deng et al., "Characteristics of high-power partially coherent laser beams propagating upwards in the turbulent atmosphere," *Opt. Express* **28**, 27927–27939 (2020).
12. D. Kip et al., "Modulation instability and pattern formation in spatially incoherent light beams," *Science* **290**, 495–498 (2000).
13. X. Zhu et al., "Generation of stochastic structured light beams with controllable beam parameters," *ACS Photonics* **10**, 2272–2279 (2022).
14. C. Vanneste, P. Sebbah, and H. Cao, "Lasing with resonant feedback in weakly scattering random systems," *Phys. Rev. Lett.* **98**, 143902 (2007).
15. D. Li and D. Pacifici, "Strong amplitude and phase modulation of optical spatial coherence with surface plasmon polaritons," *Sci. Adv.* **3**, e1700133 (2017).
16. L. Liu et al., "Spatial coherence manipulation on the disorder-engineered statistical photonic platform," *Nano Lett.* **22**, 6342–6349 (2022).
17. M. Koivurova et al., "Coherence switching with metamaterials," *Phys. Rev. Lett.* **127**, 153902 (2021).
18. Y. Shen et al., "Optical vortices 30 years on: OAM manipulation from topological charge to multiple singularities," *Light Sci. Appl.* **8**, 90 (2019).
19. I. Nape et al., "Revealing the invariance of vectorial structured light in complex media," *Nat. Photonics* **16**, 538–546 (2022).

20. K. Singh et al., "A robust basis for multi-bit optical communication with vectorial light," *Laser Photonics Rev.* **17**, 2200844 (2023).
21. A. Klug, C. Peters, and A. Forbes, "Robust structured light in atmospheric turbulence," *Adv. Photonics* **5**, 016006 (2023).
22. Z. Yang et al., "Digital spiral object identification using random light," *Light Sci. Appl.* **6**, e17013 (2017)
23. L. Waller, G. Situ, and J. W. Fleischer, "Phase-space measurement and coherence synthesis of optical beams," *Nat. Photonics* **6**, 474–479 (2012).
24. Y. Shao et al., "Spatial coherence measurement and partially coherent diffractive imaging using self-referencing holography," *Opt. Express* **26**, 4479–4490 (2018).
25. Z. Huang et al., "Measuring complex degree of coherence of random light fields with generalized Hanbury Brown–Twiss experiment," *Phys. Rev. Appl.* **13**, 044042 (2020).
26. H. Gamo, "Thermodynamic entropy of partially coherent light beams," *J. Phys. Soc. Jpn.* **19**, 1955–1961 (1964).
27. K. Kim, D. Y. Park, and J. G. Kim, "Entropic measure of global coherence of a fluctuating field," *J. Korean Phys. Soc.* **35**, 186–189 (1999).
28. M. Harling et al., "Reversible inter-degree-of-freedom optical-coherence conversion via entropy swapping," *Opt. Express* **30**, 29584–29597 (2022).
29. M. Harling et al., "Locked entropy in partially coherent optical fields," *Phys. Rev. A* **109**(2), L021501 (2024).
30. C. Okoro et al., "Demonstration of an optical-coherence converter," *Optica* **4**, 1052–1058 (2017).
31. X. Lu et al., "Four-dimensional experimental characterization of partially coherent light using incoherent modal decomposition," *Nanophotonics* **12**, 3463–3470 (2023).
32. F. Gori et al., "Beam coherence-polarization matrix," *Pure Appl. Opt.* **7**, 941 (1998).
33. F. Gori et al., "Coherent-mode decomposition of partially polarized, partially coherent sources," *J. Opt. Soc. Am. A* **20**, 78–84 (2003).
34. J. H. Eberly, X. F. Qian, and A. N. Vamivakas, "Polarization coherence theorem," *Optica* **4**, 1113–1114 (2017).
35. B. L. Moisewitsch, *Integral Equations*, Courier Corporation (2011).
36. F. Wang et al., "Three modal decompositions of Gaussian Schell-model sources: comparative analysis," *Opt. Express* **29**, 29676–29689 (2021).
37. R. French, S. Gigan, and O. L. Muskens, "Speckle-based hyperspectral imaging combining multiple scattering and compressive sensing in nanowire mats," *Opt. Lett.* **42**, 1820–1823 (2017).
38. M. Mazilu et al., "Random super-prism wavelength meter," *Opt. Lett.* **39**, 96–99 (2014).
39. F. Wang and O. Korotkova, "Convolution approach for beam propagation in random media," *Opt. Lett.* **41**, 1546–1549 (2016).
40. L. Chen, "Quantum discord of thermal two-photon orbital angular momentum state: mimicking teleportation to transmit an image," *Light Sci. Appl.* **10**, 148 (2021).
41. A. Chong et al., "Generation of spatiotemporal optical vortices with controllable transverse orbital angular momentum," *Nat. Photonics* **14**, 350–354 (2020).
42. G. Gibson et al., "Free-space information transfer using light beams carrying orbital angular momentum," *Opt. Express* **12**, 5448–5456 (2004).
43. H. Brug, "Efficient Cartesian representation of Zernike polynomials in computer memory," *Proc. SPIE* **3190**, 382–392 (1997).
44. X. Fang, H. Ren, and M. Gu, "Orbital angular momentum holography for high-security encryption," *Nat. Photonics* **14**, 102–108 (2020).
45. L. Gong et al., "Optical orbital-angular-momentum-multiplexed data transmission under high scattering," *Light Sci. Appl.* **8**, 27 (2019).
46. Y. Zhang et al., "Generating a twisted Gaussian Schell-model beam with a coherent-mode superposition," *Opt. Express* **29**, 41964–41974 (2021).
47. J. Miao et al., "Phase retrieval of diffraction patterns from noncrystalline samples using the oversampling method," *Phys. Rev. B* **67**, 174104 (2003).
48. A. Rana et al., "Potential of attosecond coherent diffractive imaging," *Phys. Rev. Lett.* **125**, 086101 (2020).
49. E. Wolf, "New spectral representation of random sources and of the partially coherent fields that they generate," *Opt. Commun.* **38**, 3–6 (1981).
50. A. Starikov and E. Wolf, "Coherent-mode representation of Gaussian Schell-model sources and of their radiation fields," *J. Opt. Soc. Am.* **72**, 923–928 (1982).

Xingyuan Lu is a postdoctoral fellow at Soochow University, collaborating with Prof. Chengliang Zhao. She received her BSc and PhD degrees from Soochow University in 2014 and 2021, respectively. From 2019 to 2021, she worked as a visiting PhD with Prof. John (Jianwei) Miao at the University of California, Los Angeles. Her main research interests are light manipulation, optical field with topology/vortex, and coherent diffraction imaging.

Zhuoyi Wang received his MSc degree in the School of Physical Science and Technology at Soochow University, China, in 2022. He is now a PhD candidate in the School of Physical Science and Technology at Soochow University, under the supervision of Prof. Chengliang Zhao. His research is mainly focused on the development of statistical optics and orbital angular momentum with their applications.

Qiwen Zhan received his PhD in electrical and computer engineering from the University of Minnesota. He is currently the principal investigator of Nano-photonics Research Group at the University of Shanghai for Science and Technology.

Yangjian Cai is a professor at the School of Physics and Electronics, Shandong Normal University, Jinan, China. He received his BSc in physics at Zhejiang University, his PhD in physics at Zhejiang University, and his PhD in electromagnetic theory at Royal Institute of Technology. His research interests include light manipulation and applications, optical coherence and polarization, atmospheric optics, laser physics, and optical imaging.

Chengliang Zhao is a professor at the School of Physical Science and Technology, Soochow University, China. He received his PhD in physics from Zhejiang University. His research interests include coherent optics, diffractive imaging, phase retrieval, and optical tweezers.